nature

THE INTERNATIONAL WEEKLY JOURNAL OF SCIENCE

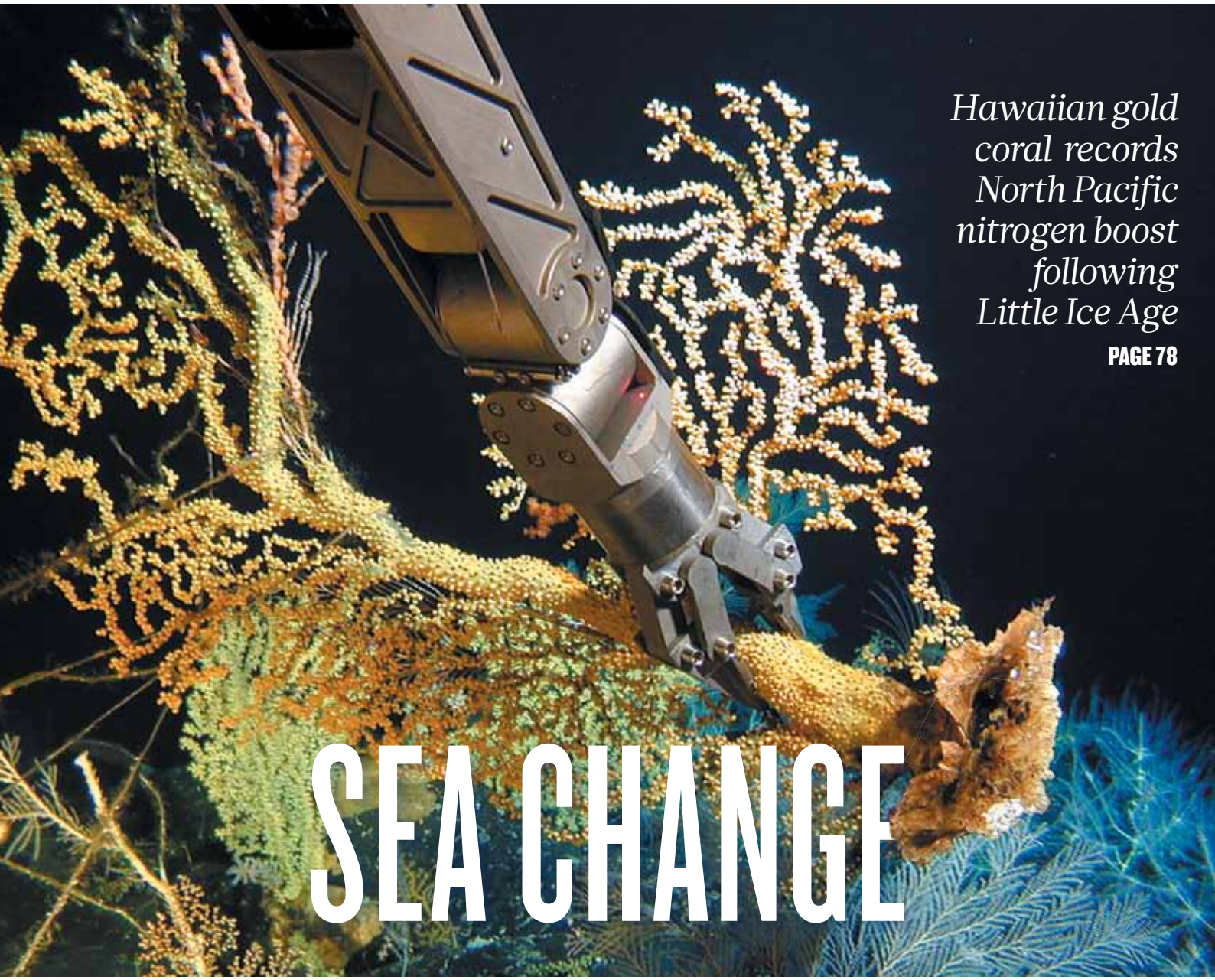

Hawaiian gold coral records North Pacific nitrogen boost following Little Ice Age

PAGE 78

SEA CHANGE

BEHAVIOURAL SCIENCE

TAMING AGGRESSION

Searching for the roots of violence in epigenetics

PAGE 14

CULTURE

THIS YEAR'S HOT TICKETS

What to see and where to be seen in 2014

PAGE 22

HUMAN EVOLUTION

NEANDERTHAL WOMAN

A complete genome sequence from Denisova cave

PAGES XX & 43

NATURE.COM/NATURE

2 January 2014 £10

Vol. 505, No. 7481

9 770028 083095 28

LETTER

doi:10.1038/nature12784

Increasing subtropical North Pacific Ocean nitrogen fixation since the Little Ice Age

Owen A. Sherwood[1]†, Thomas P. Guilderson[1,2,3], Fabian C. Batista[1], John T. Schiff[1] & Matthew D. McCarthy[1]

The North Pacific subtropical gyre (NPSG) plays a major part in the export of carbon and other nutrients to the deep ocean[1]. Primary production in the NPSG has increased in recent decades despite a reduction in nutrient supply to surface waters[2,3]. It is thought that this apparent paradox can be explained by a shift in plankton community structure from mostly eukaryotes to mostly nitrogen-fixing prokaryotes[2–4]. It remains uncertain, however, whether the plankton community domain shift can be linked to cyclical climate variability or a long-term global warming trend[5]. Here we analyse records of bulk and amino-acid-specific $^{15}N/^{14}N$ isotopic ratios ($\delta^{15}N$) preserved in the skeletons of long-lived deep-sea proteinaceous corals collected from the Hawaiian archipelago; these isotopic records serve as a proxy for the source of nitrogen-supported export production through time. We find that the recent increase in nitrogen fixation is the continuation of a much larger, centennial-scale trend. After a millennium of relatively minor fluctuation, $\delta^{15}N$ decreases between 1850 and the present. The total shift in $\delta^{15}N$ of −2 per mil over this period is comparable to the total change in global mean sedimentary $\delta^{15}N$ across the Pleistocene–Holocene transition, but it is happening an order of magnitude faster[6]. We use a steady-state model and find that the isotopic mass balance between nitrate and nitrogen fixation implies a 17 to 27 per cent increase in nitrogen fixation over this time period. A comparison with independent records[7,8] suggests that the increase in nitrogen fixation might be linked to Northern Hemisphere climate change since the end of the Little Ice Age.

Recent satellite observations have shown that globally, the permanently oligotrophic subtropical gyres are expanding at a rate of 1% to 4% per year, generally commensurate with global decreases in net primary productivity[5,9]. In contrast to the global trend, primary production in the NPSG (Fig. 1) has actually increased in recent decades, even as surface waters have become more nutrient-limited[2,3] (Extended Data Fig. 1; Extended Data Table 1). Nitrogen (N_2)-fixing prokaryotes, which use the inexhaustible supply of dissolved N_2 in surface waters, are a key factor in this apparent paradox[4]. This increase in productivity has been accompanied by a 'domain shift' from a dominantly eukaryotic to dominantly prokaryotic plankton community[2]. Such ecosystem shifts, with their impact on the export of nutrients to the deep ocean[10] and their sensitivity to past and future climate change, represent major unresolved problems in ocean and global biogeochemical cycles[11,12].

Oceanographic monitoring at station ALOHA (22° 45′ W, 158° W; Fig. 1) in the NPSG has suggested a new theory about the dynamic nature of subtropical ocean gyres on seasonal to decadal timescales. Although the NPSG was once considered static and largely unresponsive to climate forcing, it is now apparent that its physical and biological oceanographic variability may be coupled to cyclical climate phenomena such as the North Pacific Gyre Oscillation[3,13]. Therefore, it is not clear whether recent observed changes in subtropical gyre areal extent or the plankton community domain shift at station ALOHA are the result of cyclic, or anomalous (global warming) climate forcing[5]. It is thus imperative to understand these processes over longer timescales than are currently available from the observational record. However,

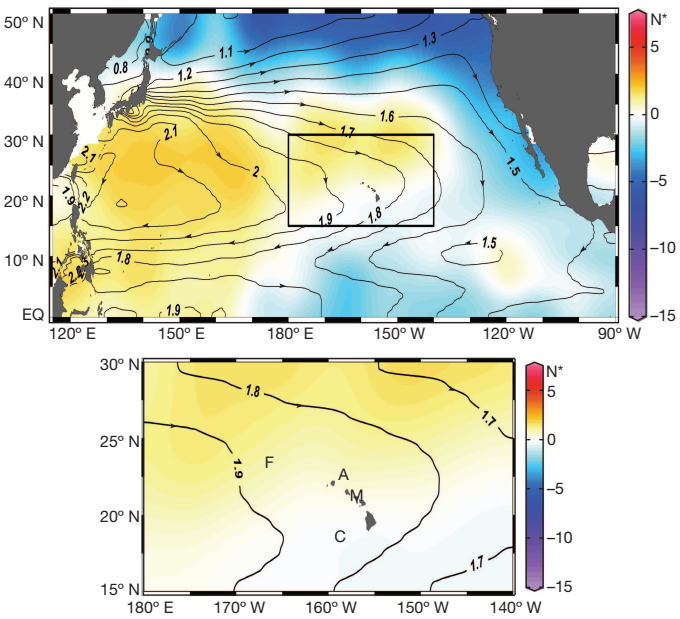

Figure 1 | NPSG circulation and N* distribution with sample locations. Contours show climatological mean dynamic height (in units of $m^2 \cdot s^{-2}$ relative to the 1,000-dbar level) with arrows showing direction of geostrophic flow. The anticyclonic NPSG lies approximately west of the 1.6 $m^2 s^{-2}$ contour, between 10° N and 40° N. The colour scale shows the distribution of N* (N* = N − 16P + 2.9 μmol kg^{-1}, where P is phosphorus) (ref. 30). Positive N* indicates where the oceanic N inventory is increased by N_2 fixation; negative N* indicates where nitrogen is lost to water column denitrification. The lower panel shows *K. haumeaae* sampling locations—Cross Seamount (C), Makapuu (M) and French Frigate Shoals (F)—and the location of oceanographic station ALOHA (A).

traditional palaeo-archives from sediment cores cannot provide meaningful longer-term context, because the entire Holocene history of the NPSG is represented in less than 10 cm of bioturbated sediment.

Here, we use the unique geochemical time-series data encoded in the skeletons of extraordinarily long-lived, deep-sea corals to reconstruct the first detailed biogeochemical proxy records of the NPSG. The Hawaiian gold coral *Kulamanamana haumeaae* Sinniger *et al.*, 2013 (previously known as *Gerardia* sp.), secretes a proteinaceous skeleton synthesized from its primary food source: recently exported sinking particles[14]. These growth-layered, decay-resistant skeletons therefore record the biogeochemical signatures of exported production, in a manner analogous to 'living sediment traps', with annual- to decadal-scale resolution over millennial timescales[14,15].

We have generated records of skeletal bulk $\delta^{15}N$ ($\delta^{15}N_{bulk}$) from specimens of *K. haumeaae* collected from three sites in the Hawaiian archipelago (Fig. 1). These records all show that from around 1000 AD to 1850 AD, $\delta^{15}N_{bulk}$ showed no long-term, secular trend (Fig. 2a). Then, beginning around the end of the Little Ice Age (around 1850 AD), $\delta^{15}N_{bulk}$

[1]Ocean Sciences Department, University of California, Santa Cruz, California 95064, USA. [2]Lawrence Livermore National Laboratory, Livermore, California 94550, USA. [3]Institute for Marine Sciences, University of California, Santa Cruz, California 95064, USA. †Present address: Institute of Arctic and Alpine Research, University of Colorado, Boulder, Colorado 80309, USA.

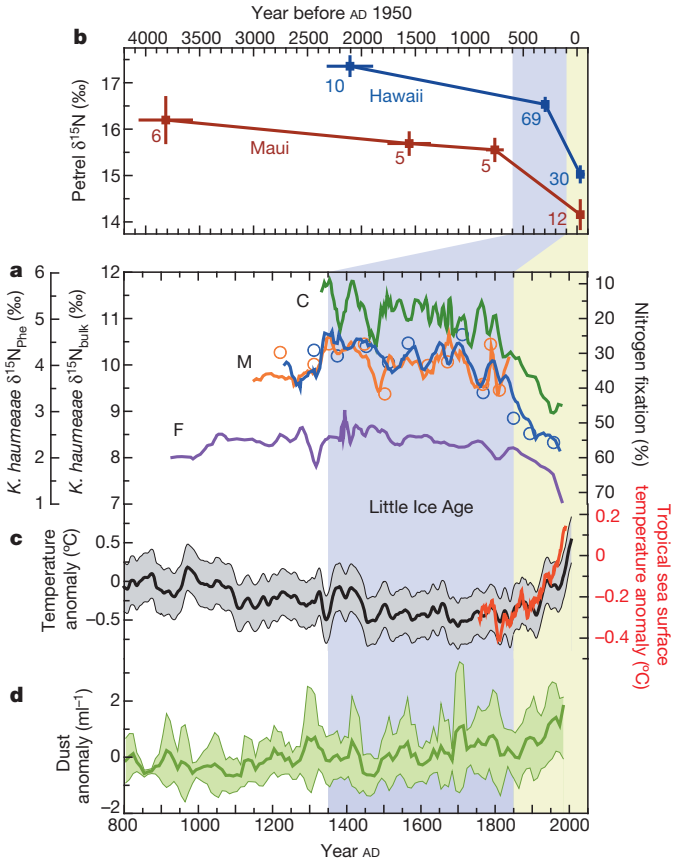

Figure 2 | NPSG $\delta^{15}N$ proxy records and their relationship to climate change. **a**, Records of *K. haumeaae* $\delta^{15}N_{bulk}$ (solid lines show the three-point running average, analytical error <0.15‰) and $\delta^{15}N_{Phe}$ (corresponding orange and blue circles, analytical error <1.0‰). Abbreviations (M, C, F) as in Fig. 1. Percentage N_2-fixation based on mixing between NO_3^- and N_2-fixation shown on separate axis. **b**, Petrel bone collagen $\delta^{15}N$ records[17]. For clarity, records are shown for Hawaii and Maui breeding populations only. Error bars are 1 s.e.m., with sample size indicated. **c**, Northern Hemisphere temperature reconstruction[8] (black line with 95% confidence envelope) and tropical Pacific sea surface temperature reconstruction[7] (red line). **d**, Composite dust record from Himalayan ice cores[29] (green line with 95% confidence envelope).

began to decrease dramatically and monotonically to levels not seen at any point over the mid- to late Holocene epoch[16]. The timing and magnitude of the decrease in $\delta^{15}N_{bulk}$ is similar to recently reported records of $\delta^{15}N$ preserved in the bone collagen of Hawaiian petrels (*Pterodroma sandwichensis*)[17] (Fig. 2b), suggesting that the observed changes in $\delta^{15}N$ are linked across multiple trophic levels. The most recent parts of these records overlap with instrumental data, over which time the NPSG has become increasingly nutrient-limited and more favourable to N_2-fixing diazotrophs (Extended Data Fig. 1; Extended Data Table 1).

Values of $\delta^{15}N_{bulk}$ can be difficult to interpret directly: bulk values represent the effects of baseline nitrogen-source signatures combined with subsequent alterations due to trophic transfer[18]. Recently, analysis of the $\delta^{15}N$ of individual amino acids ($\delta^{15}N_{aa}$) has emerged as a powerful new tool with which to decouple and unambiguously examine these effects independently of one other[15,18–20]. In heterotrophic organisms, amino acids fall into two isotopically distinct groups[18,21] (Extended Data Fig. 2). One group, the 'source' amino acids (SrcAA in Table 1), remain little changed through successive trophic levels of a food web. In contrast, 'trophic' amino acids (TrAA in Table 1) become significantly enriched in ^{15}N with each successive trophic transfer.

To distinguish between the effects of baseline nitrogen-source signatures from subsequent trophic alterations, we measured $\delta^{15}N_{aa}$ on a subset of the samples spanning the bulk records. The values for individual

Table 1 | Correlation of $\delta^{15}N_{aa}$ parameters with $\delta^{15}N_{bulk}$

	Parameter	Slope	Standard error	r^2	*P* value
SrcAA	Gly	0.99	0.31	0.36	**0.005**
	Ser	1.10	0.34	0.36	**0.005**
	Lys	0.88	0.19	0.56	**<0.001**
	Tyr	0.76	0.31	0.27	**0.026**
	Phe	1.06	0.13	0.80	**<0.001**
	Average SrcAA	1.00	0.13	0.78	**<0.001**
TrAA	Glx	0.92	0.43	0.20	**0.049**
	Asx	0.76	0.26	0.32	**0.009**
	Ala	0.97	0.42	0.23	**0.034**
	Ile	1.37	0.37	0.44	**0.002**
	Leu	0.94	0.33	0.30	**0.012**
	Pro	0.80	0.29	0.29	**0.014**
	Val	0.51	0.32	0.13	0.126
	Average TrAA	0.88	0.23	0.46	**0.001**
	Trophic position (average TrAA minus average SrcAA)	-0.01	0.03	0.00	0.880
	Trophic position (Glu minus Phe method)	-0.04	0.06	0.02	0.545
	ΣV	0.04	0.12	0.01	0.724

Boldface indicates significant correlations at the $P < 0.05$ level. Strong correlations are seen for individual source amino acids (SrcAA) and trophic amino acids (TrAA), including overall SrcAA and TrAA group averages. Estimates of trophic position, calculated using two different formulations, as well as microbial resynthesis (as indicated by the ΣV parameter) were uncorrelated with $\delta^{15}N_{Bulk}$ ($n = 20$). This indicates that trends in $\delta^{15}N_{bulk}$ timeseries are driven by $\delta^{15}N$ at the base of the foodweb. Source amino acids are glycine (Gly), serine (Ser), lysine (Lys), tyrosine (Tyr) and phenylalanine (Phe). Trophic amino acids are glutamic acid + glutamine (Glx), aspartic acid + asparagine (Asx), alanine (Ala), isoleucine (Ile), leucine (Leu), proline (Pro) and valine (Val). The two relative trophic position formulations were: $\{[(\delta^{15}N_{average\ TrAA} - \delta^{15}N_{average\ SrcAA}) - 3.4]/7.6\} + 1$ (ref. 19) and $\{[(\delta^{15}N_{Glu} - \delta^{15}N_{Phe}) - 3.4]/7.6\} + 1$ (ref. 19). $\Sigma V = 1/7\Sigma Abs(\delta^{15}N_{TrAA} - \delta^{15}N_{average\ TrAA})$ (ref. 19).

amino acids, as well as SrcAA and TrAA group averages, were significantly correlated with $\delta^{15}N_{bulk}$, with a slope near unity (Table 1). In contrast, calculated trophic position remained essentially constant, and had no statistical relationship with $\delta^{15}N_{bulk}$. This implies that most of the variability in $\delta^{15}N_{bulk}$ (Fig. 2a) can be attributed to changes in source nitrogen at the base of the foodweb. Among the SrcAA group, phenylalanine (Phe) best preserves the baseline $\delta^{15}N$ values, with negligible fractionation through trophic transfers in planktonic food webs[18,21]. In the Makapuu corals (Fig. 1), $\delta^{15}N_{Phe}$ decreased from an average of 4.1 ± 0.4‰ (1 s.d., $n = 16$) during the pre-1850 period, to a low of 2.3‰ in the most recent part of the record (Fig. 2a). This latter value is directly within the range of present-day thermocline NO_3^- ($\delta^{15}N_{NO3} = 1.5$–2.4‰, $n = 4$) and sinking particulate nitrogen ($\delta^{15}N_{pNsink} = 2.3$–3.6‰, $n = 6$) at station ALOHA[22] (Fig. 3), confirming that $\delta^{15}N_{Phe}$ in these corals represents a close proxy for baseline $\delta^{15}N$ values (Methods). Further, both the $\delta^{15}N_{aa}$ patterns and the analysis of the $\delta^{15}N$ of TrAA confirm that neither trophic position nor the microbial resynthesis of sinking particles has significantly affected the observed trends in $\delta^{15}N_{bulk}$ (Table 1, Extended Data Fig. 3).

On the multi-decadal timescale of the observed trends (Fig. 2a), exported productivity in the NSPG is supported by two isotopically distinct nitrogen sources: fixation of dissolved N_2 ($\delta^{15}N_{Nfix} = -1$‰), and upward transport of NO_3^- ($\delta^{15}N_{NO3} = 6.5$‰)[4,22,23]. Assuming that inputs of N must be balanced by exports of sinking particulate nitrogen, the proportional contribution of each source is reflected in $\delta^{15}N_{pNsink}$[4,22,23]. Therefore, a well-established, two-endmember mixing model—$F_{Nfix} = 1 - [(\delta^{15}N_{pNsink} - \delta^{15}N_{Nfix})/(\delta^{15}N_{NO3} - \delta^{15}N_{Nfix})]$, where F_{Nfix} is the fraction of N_2 fixation—has been widely applied to estimate the contribution of N_2 fixation to export production at station ALOHA (that is, about half at present)[4,10,13,22,23]. By substituting coral $\delta^{15}N$ as a proxy for $\delta^{15}N_{pNsink}$, the long-term change in N_2 fixation may be estimated. Using this simple model, the change observed in the Makapuu and Cross Seamount records ($\Delta\delta^{15}N_{bulk} = \Delta\delta^{15}N_{Phe} = -2$‰) indicates a 27% increase in N_2 fixation since about 1850 AD. For French Frigate Shoals ($\Delta\delta^{15}N_{bulk} = -1.3$‰) the same calculation indicates a 17% increase. We note that the addition or modification of nitrogen-isotope endmembers could potentially affect this interpretation; however,

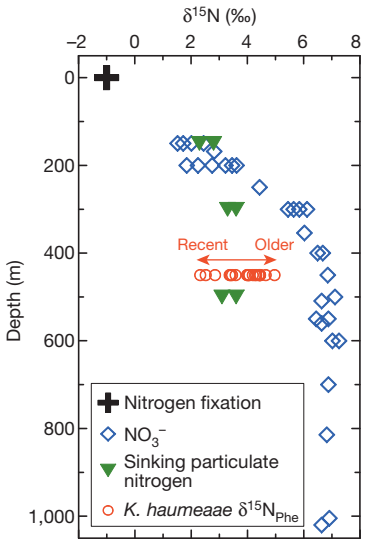

Figure 3 | Depth variations in water column $\delta^{15}N$ confirm *K. haumeaa* $\delta^{15}N_{Phe}$ as a proxy for export production. Particulate nitrogen export at station ALOHA is supported by N_2 fixation and the upward flux of deep (>400 m) NO_3^-. Remineralization of sinking particulate nitrogen contributes to formation of a shallow (150–300 m) pool of isotopically light (~2.5‰) NO_3^-, which turns over in less than 15 years (ref. 22). Makapuu *K. haumeaae* $\delta^{15}N_{Phe}$ (analytical error <1.0‰) decreased from an average of 4.2‰ before about 1850, to a low of 2.3‰ in the late twentieth century (red arrow), within range of the shallow $\delta^{15}N_{NO3}$ and sinking particles[22].

none of the plausible mechanisms, such as atmospheric or land-based sources of nitrogen or changes in eastern Pacific denitrification, can explain the observed trends (Methods).

We offer two hypotheses for the long-term increase in N_2 fixation indicated by the *K. haumeaae* records. The first involves a sustained expansion of the NPSG since the end of the Little Ice Age. This idea is supported by current seasonal trends in the NSPG extent and N_2 fixation, as well as the $\delta^{15}N_{bulk}$ offsets between sampling locations with respect to the distribution of the nitrogen-to-phosphorus (P) stoichiometric imbalance parameter N* (where $N^* = N - 16P + 2.9\ \mu mol\ kg^{-1}$) (ref. 30) (Fig. 1). Currently, seasonal fluctuations in gyre areal extent and nutrient inventories are associated with predictable changes in both N_2 fixation[13,24] and the $\delta^{15}N$ of export production: at station ALOHA, the larger summertime gyre corresponds with an approximately 1.5‰ decrease in $\delta^{15}N_{pNsink}$ (refs 10, 23). Such seasonal changes provide a model for how N_2 fixation and $\delta^{15}N_{pNsink}$ might change with progressive gyre expansion over a longer timescale. Further, the relative offsets in the $\delta^{15}N_{bulk}$ records between our three locations, as well as the relative gradients of change observed (Fig. 2a), are also consistent with an expanding gyre margin. Finally, longer-term expansion of NPSG on multiple timescales has also been inferred from satellite imagery[5,9,25], models[5], and direct observation records[2,3] (Extended Data Fig. 1; Extended Data Table 1). Although recent shifts could also be related to interannual to decadal natural cycles[3,5,13], a number of centennial-scale trends, including decreased precipitation[26], increased tropical Pacific sea surface temperature[7] (Fig. 2b) and inferred shifts in the latitudinal position of the Pacific intertropical convergence zone after the Little Ice Age[27], are all consistent with the idea of NPSG expansion.

A second hypothesis involves an increase in N_2 fixation linked to the supply of iron-bearing dust aerosols[11]. Hawaii is significantly affected by bioavailable iron dust originating from Asia, which relaxes the iron limitation for N_2-fixing diazotrophs[28]. Millennial-length ice-core records from Himalayan glaciers document up to fourfold increases in dust concentrations over the past century, reflecting warming trends in Asia[29] (Fig. 2c). Such an increase might also account for the trend towards higher rates of N_2 fixation indicated by the *K. haumeaae* $\delta^{15}N$ records. However, neither gyre expansion or increasing dust deposition are mutually exclusive hypotheses, and we note that ultimately both are the result of a common driver—the Northern Hemisphere warming trends since the end of the Little Ice Age[8].

Overall, these data provide strong evidence for a progressive, 17%–27% increase in N_2 fixation in the NPSG since the mid-nineteenth century, unique with respect to the mid- to late Holocene and comparable in magnitude to the total change in global mean sedimentary $\delta^{15}N$ across the Pleistocene–Holocene transition[6]. From a consideration of the mechanisms that can most plausibly explain this shift, we conclude that export productivity in the NPSG has been responding to anomalous climate forcing over the past 150 years or so.

Given that the *K. haumeaae* records are a proxy for exported productivity, these data indicate that the biogeochemical impacts of changing surface N_2 fixation propagate at least into the mesopelagic ocean on centennial timescales. This signal, in both timing and amplitude, is propagated into multiple higher trophic levels of the marine food web and is observed in petrel bone bulk $\delta^{15}N$ data: that is, the petrel data are probably not reflecting declining trophic position[17], but instead changes at the base of the food web. These dramatic changes in the world's largest contiguous biome (NPSG) highlight the important role of nitrogen fixation in the response of marine ecosystems to long-term climate change.

METHODS SUMMARY

Colonies of Hawaiian gold coral (*K. haumeaae*) were collected from water depths of approximately 450 m with the HURL/NOAA *Pisces V* submersible between 1997 and 2004 (ref. 14 and Extended Data Fig. 4). Air-dried colonies were sectioned near the skeletal base, polished and photographed under a binocular microscope. A computerized Merchantek micromill was used to mill samples, parallel to growth banding, at increments of 0.1 mm, along radial transects from the outer edge to the centre of each section (Extended Data Fig. 5). Each sample represents from 1 to 20 (average 5) years of growth, depending on growth rate. Radiocarbon dating of sample aliquots (Extended Data Table 2) was used for age modelling (Extended Data Fig. 6).

Bulk $\delta^{15}N$ isotope ratios—defined as $\delta^{15}N = [(^{15}N/^{14}N)_{sample}/(^{15}N/^{14}N)_{standard} - 1] \times 1{,}000$—were measured using a Carlo Erba 1108 elemental analyser interfaced to a ThermoFinningan Delta Plus XP isotope ratio mass spectrometer (IRMS). Values are reported in per mil (‰) units relative to atmospheric N_2 ($\delta^{15}N_{air} = 0$‰). Reproducibility, as measured by the difference in sample replicates, averaged <0.15‰.

Amino-acid-specific $\delta^{15}N_{aa}$ was measured on sample composites (combining 3 to 10 separate samples to obtain a total mass of 15–20 mg). Composites were hydrolysed in 100 ml of 6 N HCl for 20 h, and spiked with a norleucine internal standard followed by formation of trifluoroacetyl/isopropyl ester derivatives[19]. These derivatives were analysed on a Thermo Trace Ultra gas chromatograph, fitted with a SGE BPX5 capillary column (60 m × 0.32 mm internal diameter, 1 μm film thickness), in line with the oxidation and reduction furnaces, and linked to a ThermoFinnigan Delta Plus XP IRMS. Samples were analysed in quadruplicate. Analytical accuracy was monitored by analysis of the norleucine internal standard and co-derivatized amino-acid external standards for which authentic $\delta^{15}N$ values of each amino acid were determined offline. Reproducibility for individual amino-acid values was typically better than 1‰.

Online Content Any additional Methods, Extended Data display items and Source Data are available in the online version of the paper; references unique to these sections appear only in the online paper.

Received 2 February; accepted 2 October 2013.
Published online 15 December 2013.

1. Emerson, S. *et al.* Experimental determination of the organic carbon flux from open-ocean surface waters. *Nature* **389,** 951–954 (1997).
2. Karl, D. M., Bidigare, R. R. & Letelier, R. M. Long-term changes in plankton community structure and productivity in the North Pacific Subtropical Gyre: the domain shift hypothesis. *Deep Sea Res. Part II* **48,** 1449–1470 (2001).
3. Corno, G. *et al.* Impact of climate forcing on ecosystem processes in the North Pacific Subtropical Gyre. *J. Geophys. Res.* **112,** C04021 (2007).
4. Karl, D. *et al.* The role of nitrogen fixation in biogeochemical cycling in the subtropical North Pacific Ocean. *Nature* **388,** 533–538 (1997).
5. Henson, S. A. *et al.* Detection of anthropogenic climate change in satellite records of ocean chlorophyll and productivity. *Biogeosciences* **7,** 621–640 (2010).
6. Galbraith, E. D. *et al.* The acceleration of oceanic denitrification during deglacial warming. *Nature Geosci.* **6,** 579–584 (2013).
7. Wilson, R. *et al.* Two-hundred-fifty years of reconstructed and modeled tropical temperatures. *J. Geophys. Res.* **111,** C10007 (2006).

8. Mann, M. E. *et al.* Proxy-based reconstructions of hemispheric and global surface temperature variations over the past two millennia. *Proc. Natl Acad. Sci. USA* **105,** 13252–13257 (2008).
9. Polovina, J. J., Howell, E. A. & Abecassis, M. Ocean's least productive waters are expanding. *Geophys. Res. Lett.* **35,** L03618 (2008).
10. Karl, D. M., Church, M. J., Dore, J. E., Letelier, R. M. & Mahaffey, C. Predictable and efficient carbon sequestration in the North Pacific Ocean supported by symbiotic nitrogen fixation. *Proc. Natl Acad. Sci. USA* **109,** 1842–1849 (2012).
11. Falkowski, P. G., Barber, R. T. & Smetacek, V. Biogeochemical controls and feedbacks on ocean primary production. *Science* **281,** 200–206 (1998).
12. Chavez, F. P., Messie, M. & Pennington, J. T. Marine primary production in relation to climate variability and change. *Annu. Rev. Mar. Sci.* **3,** 227–260 (2011).
13. Dave, A. C. & Lozier, M. S. Local stratification control of marine productivity in the subtropical North Pacific. *J. Geophys. Res.* **115,** C12032 (2010).
14. Roark, E. B., Guilderson, T. P., Dunbar, R. B., Fallon, S. J. & Mucciarone, D. A. Extreme longevity in proteinaceous deep-sea corals. *Proc. Natl Acad. Sci. USA* **106,** 5204–5208 (2009).
15. Sherwood, O. A., Lehmann, M. F., Schubert, C. J., Scott, D. B. & McCarthy, M. D. Nutrient regime shift in the western North Atlantic indicated by compound-specific δ^{15}N of deep-sea gorgonian corals. *Proc. Natl Acad. Sci. USA* **108,** 1011–1015 (2011).
16. Guilderson, T. P., McCarthy, M. D., Dunbar, R. B., Englebrecht, A. & Roark, E. B. Late Holocene variations in Pacific surface circulation and biogeochemistry inferred from proteinaceous deep-sea corals. *Biogeosciences* **10,** 6019–6028 (2013).
17. Wiley, A. E. *et al.* Millenial-scale isotope records from a wide-ranging predator show evidence of recent human impact to oceanic food webs. *Proc. Natl Acad. Sci. USA* **110,** 8972–8977 (2013).
18. McClelland, J. W. & Montoya, J. P. Trophic relationships and the nitrogen isotopic composition of amino acids in plankton. *Ecology* **83,** 2173–2180 (2002).
19. McCarthy, M. D., Benner, R., Lee, C. & Fogel, M. L. Amino acid nitrogen isotopic fractionation patterns as indicators of heterotrophy in plankton, particulate, and dissolved organic matter. *Geochim. Cosmochim. Acta* **71,** 4727–4744 (2007).
20. Popp, B. N. *et al.* Insight into the trophic ecology of yellowfin tuna, *Thunnus albacares*, from compound-specific nitrogen isotope analysis of proteinaceous amino acids. *Terr. Ecol.* **1,** 173–190 (2007).
21. Chikaraishi, Y. *et al.* Determination of aquatic food-web structure based on compund-specific nitrogen isotopic composition of amino acids. *Limnol. Oceanogr. Methods* **7,** 740–750 (2009).
22. Casciotti, K. L., Trull, T. W., Glover, D. M., &. Davies, D. Constraints on nitrogen cycling at the subtropical North Pacific Station ALOHA from isotopic measurements of nitrate and particulate nitrogen. *Deep Sea Res. Part II* **55,** 1661–1672 (2008).
23. Dore, J. E. Brum, J. R., Tupas, L. M. & Karl, D. M. Seasonal and interannual variability in sources of nitrogen supporting export in the oligotrophic subtropical North Pacific Ocean. *Limnol. Oceanogr.* **47,** 1595–1607 (2002).
24. Church, M. J. *et al.* Physical forcing of nitrogen fixation and diazotroph community structure in the North Pacific subtropical gyre. *Glob. Biogeochem. Cycles* **23,** GB2020 (2009).
25. Behrenfeld, M. J. *et al.* Climate-driven trends in contemporary ocean productivity. *Nature* **444,** 752–755 (2006).
26. Diaz, H. F. & Giambelluca, T. W. Changes in atmospheric circulation patterns associated with high and low rainfall regimes in the Hawaiian Islands region on multiple timescales. *Glob. Planet. Change* **98–99,** 97–108 (2012).
27. Sachs, J. P. *et al.* Southward movement of the Pacific intertropical convergence zone AD 1400–1850. *Nature Geosci.* **2,** 519–525 (2009).
28. Boyle, E. A., Bergquist, B. A., Kayser, R. A. & Mahowald, N. Iron, manganese, and lead at Hawaii Ocean Time-series station ALOHA: temporal variability and an intermediate water hydrothermal plume. *Geochim. Cosmochim. Acta* **69,** 933–952 (2005).
29. Thompson, L. G. *et al.* A high-resolution millenial record of the South Asian monsoon from Himalayan ice cores. *Science* **289,** 1916–1919 (2000).
30. Deutsch, C., Gruber, N., Key, R. M., Sarmiento, J. L. & Ganachaud, A. Denitrification and N_2 fixation in the Pacific Ocean. *Glob. Biogeochem. Cycles* **15,** 483–506 (2001).

Acknowledgements We thank the captain and crew of the RV *Ka'imikai-o-Kanaloa* and the pilots and engineers of the Hawaiian Undersea Research Laboratory's *Pisces V* submersible for their assistance in collecting the specimens presented here. Funding for sample collection was from NOAA/NURP and the National Geographic Society (grant number 7717-04). Radiocarbon analyses were performed under the auspices of the US Department of Energy (grant number DE-AC52-07NA27344). The bulk of the work presented here was funded by the NSF (grant number OCE 1061689).

Author Contributions O.A.S. helped conceive the project, prepared samples, performed bulk and compound-specific δ^{15}N analyses and wrote the paper. F.C.B. and J.T.S. assisted in sample preparation and analysis, and commented on the manuscript. T.P.G. and M.D.M. conceived and supervised this project, discussed the results and edited the manuscript.

Author Information Data will be digitally archived with the National Oceanic and Atmospheric Adminstration paleoclimatology datasets (http://www.ncdc.noaa.gov/data-access/paleoclimatology-data/datasets) after publication. Reprints and permissions information is available at www.nature.com/reprints. The authors declare no competing financial interests. Readers are welcome to comment on the online version of the paper. Correspondence and requests for materials should be addressed to O.A.S. (owen.sherwood@colorado.edu).

METHODS

Sample collection and preparation. Colonies of Hawaiian gold coral were collected from water depths of approximately 450 m with the HURL/NOAA *Pisces V* submersible between 1997 and 2004 (ref. 14 and Extended Data Fig. 4). Traditionally known as *Gerardia* sp., the Hawaiian gold coral was recently reclassified as a newly erected genus and species, *Kulumanana haumeaae*[31]. All of the specimens were collected alive, with the exception of specimen Ger9702 from Makapuu which was dead when collected. Air-dried colonies were sectioned near the skeletal base with a rock saw. Sections 10 mm thick were mounted on 50 mm × 75 mm glass slides with epoxy, ground and polished on diamond laps, ultrasonically cleansed in isopropyl alcohol, and photographed under a binocular microscope. A computerized Merchantek micromill was used to mill samples, parallel to growth banding, at increments of 0.1 mm, along radial transects from the outer edge to the centre of each section (Extended Data Fig. 5). Each approximately 5-mg sample represents from 1 to 20 (average 5) years of growth, depending on growth rate.

Radiocarbon dating and age models. Radiocarbon dating was performed on 8 to 10 sample aliquots from each section of *K. haumeaae*. Radiocarbon measurements were performed at the Center for Accelerator Mass Spectrometry (CAMS), Lawrence Livermore National Laboratory. Aliquots (1 mg) were combusted in individual quartz tubes and reduced to graphite in the presence of iron catalyst. Results include a background and $\delta^{13}C$ correction and are reported as Fraction modern ^{14}C (ref. 32; Extended Data Table 2). Radiocarbon age calibrations and age models were generated with Clam version 2.0 (ref. 33), using the Marine09 database[34] with a local reservoir (ΔR) correction[35] of -34 ± 13 years, based on a chronology of surface water ^{14}C from Hawaiian reef corals[36]. Post-bomb values were calibrated directly to the Hawaiian surface water chronology[36]. Age models were fitted with a spline function with a smoothing level of 0.6. Models were run over 1,000 iterations, from which mean ages and 95% confidence levels were calculated (Extended Data Fig. 6).

Bulk N isotope analysis. $\delta^{15}N$ isotope ratios—defined as $\delta^{15}N = [(^{15}N/^{14}N)_{sample}/(^{15}N/^{14}N)_{standard} - 1] \times 1{,}000$—were measured on 0.7-mg aliquots of all the milled samples using a Carlo Erba 1108 elemental analyser interfaced to a ThermoFinningan Delta Plus XP isotope ratio mass spectrometer (IRMS). Values are reported in per mil (‰) units relative to atmospheric N_2 ($\delta^{15}N_{air} = 0$‰). Raw isotope values were corrected for instrument drift and linearity effects and calibrated against the in-house isotopic reference materials of the Stable Isotope Lab, University of California, Santa Cruz, using standard laboratory protocols (http://es.ucsc.edu/~silab/index.php). Reproducibility, as measured by the difference in sample replicates, averaged <0.15‰.

AA hydrolysis and derivitization. Sample composites (combining 3 to 10 separate samples to obtain a total mass of 15–20 mg) were hydrolysed in 100 ml of 6 N HCl for 20 h, and spiked with 6 µl of norleucine internal standard ($\delta^{15}N = 7.9$‰). Hydrolysates were evaporated to dryness under a stream of N_2 and stored in a desiccator overnight, followed by formation of trifluoroacetyl/isopropyl ester derivatives[19].

Amino-acid compositional analysis. Amino-acid molar composition was determined with an Agilent 7890A gas chromatograph fitted with a SGE BPX-5 column (60 m × 0.32 mm internal diameter, 1 µm film thickness). Response factors were determined with a dilution series of an external amino-acid standard mixture of 14 common protein amino acids. Reproducibility, as measured by the standard deviation of analytical replicates, averaged <5 mol.%. Arginine (Arg), cysteine (Cys) and histidine (His) concentrations could not be determined owing to their breakdown during acid hydrolysis.

$\delta^{15}N$ amino-acid analysis. Measurement of the $\delta^{15}N$ of amino-acid derivatives was performed using previously published procedures[19]. Derivatives were analysed on a Thermo Trace Ultra gas chromatograph, fitted with a SGE BPX5 capillary column (60 m × 0.32 mm internal diameter, 1 µm film thickness), in line with the oxidation and reduction furnaces, and linked to a ThermoFinnigan Delta Plus XP IRMS. Samples were analysed in quadruplicate. Analytical accuracy was monitored by analysis of the norleucine internal standard and co-derivatized amino-acid external standards for which authentic $\delta^{15}N$ values of each amino acid were determined offline. Reproducibility for individual amino-acid values was typically better than 1‰. The $\delta^{15}N$ of methionine (Met) was not measured owing to insufficient concentrations.

Oceanographic data. The dynamic height and N* data in Fig. 1 use gridded data from World Ocean Atlas 2009 (http://www.nodc.noaa.gov/OC5/WOA09/woa09data.html). Data in Extended Data Fig. 1 and Extended Data Table 1 use ocean station data from World Ocean Database 2009 (http://www.nodc.noaa.gov/OC5/SELECT/dbsearch/dbsearch.html) for the region 17.5–27.5° N, 150–170° W. Data were filtered for outliers and plotted using Ocean Data View software, version 4.3.10 (R. Schlitzer, http://odv.awi.de).

Climate records. Temperature record in Fig. 2c is from the NHHAD_EIV Northern Hemisphere land and ocean multiple proxy temperature reconstruction of ref. 8, smoothed with a 15-year running average. The tropical Pacific sea surface temperature record is from the compilation of reef coral oxygen isotope records of ref. 7, smoothed with a 15-year running average. The dust record in Fig. 2d is from a compilation of the Dasuopo, Dunde and Guliya Himalayan ice cores[29]. Individual decadal records were normalized by subtracting the mean and dividing by the standard deviation for each record. The composite record is the average of the three individual records, smoothed with a 20-year running average.

Deep-sea coral $\delta^{15}N$ as a proxy for sinking particulates. It has been well established that the skeletons of *K. haumeaae* and other deep-sea proteinaceous corals are biogeochemically tightly coupled to surface waters. The presence of bomb radiocarbon (that is, post-1950) signatures in the living tissues and skeletal protein of deep-sea corals establishes recently exported particles as their main food source[37]. The incorporation of detailed bomb-radiocarbon chronologies within the skeletal growth rings, without any significant attenuation or time-lag relative to surface water chronologies, further establishes that euphotic zone biogeochemical signatures are transmitted to deep-sea corals efficiently and rapidly[14,15]. The $\delta^{15}N_{Phe}$ signature in the Makapuu *K. haumeaae* specimens closely matches the $\delta^{15}N$ of both sinking particulates and thermocline NO_3^- (Fig. 3). Data from two other oceanographic regions, the northwest Atlantic and the denitrification-affected eastern north Pacific, show that coral $\delta^{15}N_{Phe}$ values closely follow the same pattern as NO_3^- with respect to N* (Extended Data Fig. 7).

Steady state isotopic mass balance model assumptions. The isotopic mass balance model assumes that the export flux of particulate N at station ALOHA and surrounding waters of the NSPG is balanced by N_2 fixation and upward flux of NO_3^- (refs 4, 10, 13, 22 and 23). There is no isotopic impact from incomplete NO_3^- assimilation, because NO_3^- in the mixed layer is exhausted to $<0.2\ \mu mol\ kg^{-1}$ year-round (Hawaii Ocean Time-series Data Organization and Graphical System (HOT-DOGS); see http://hahana.soest.hawaii.edu/hot/hot-dogs/interface.html). Additional nitrogen isotopic endmembers are negligible to the nitrogen budget. Atmospheric deposition of organic nitrogen accounts for <2% of the particulate nitrogen export at 150 m (refs 4, 23 and 30). Terrestrial runoff of fertilizers (values near −2‰) can depress local seawater $\delta^{15}N$, but the similar trends at all three locations, including French Frigate Shoals (Fig. 1), rules out any direct land-use effect from the Hawaiian islands.

Finally, modification of Pacific midwater $\delta^{15}N_{NO3}$ could arise from changes in the rates of denitrification along the eastern Pacific margin[38]. However, this is very unlikely to account for the trends in $\delta^{15}N$ of Hawaiian *K. haumeaae* (Fig. 2) for the following reasons. (1) Denitrification would have to decrease to account for the observed downward trends in *K. haumeaae* $\delta^{15}N$, whereas in fact denitrification has increased in global oxygen minimum zones, including the ETNP[39,40]. (2) The geostrophic circulation isolates the NPSG from a tongue of denitrification-affected waters, of which the northern boundary lies south of the Hawaiian archipelago at a latitude of 10° N (refs 30 and 41). (3) Oceanographic data from the Hawaiian archipelago show that oxygen levels in the upper 500 m have remained constant or have increased (Extended Data Fig. 1; Extended Data Table 1). This observation is consistent with expansion of the NPSG and inconsistent with any impact of denitrification from the eastern Pacific margin.

31. Sinniger, F., Ocana, O. V. & Baco, A. R. Diversity of zoanthids (Anthozoa: Hexacorallia) on Hawaiian seamounts: description of the Hawaiian gold coral and additional zoanthids. *PLoS ONE* **8,** e52607 (2013).
32. Stuiver, M. & Polach, H. A. Reporting of ^{14}C data. *Radiocarbon* **19,** 355–363 (1977).
33. Blaauw, M. Methods and code for 'classical' age-modelling of radiocarbon sequences. *Quat. Geochronol.* **5,** 512–518 (2010).
34. Reimer, P. J. *et al.* IntCal09 and Marine09 radiocarbon age calibration curves, 0-50,000 years cal BP. *Radiocarbon* **51,** 1111–1150 (2009).
35. Stuiver, M. & Braziunas, T. F. Modeling atmospheric ^{14}C influences and ^{14}C ages of marine samples to 10,000 BC. *Radiocarbon* **35,** 137–189 (1993).
36. Druffel, E. R. M. *et al.* Changes of subtropical North Pacific radiocarbon and correlation with climate variability. *Radiocarbon* **43,** 15–25 (2001).
37. Griffin, D. W. & Druffel, E. R. M. Sources of carbon to deep-sea corals. *Radiocarbon* **31,** 533–543 (1989).
38. Sigman, D., DiFiore, P. J., Hain, M. P., Deutsch, C. & Karl, D. M. Sinking organic matter spreads the nitrogen isotope signal of pelagic denitrification in the North Pacific. *Geophys. Res. Lett.* **36,** L08605 (2009).
39. Gutiérrez, D. *et al.* Rapid reorganization in ocean biogeochemistry off Peru towards the end of the Little Ice Age. *Biogeosciences* **6,** 835–848 (2009).
40. Stramma, L., Johnson, G. C., Sprintall, J. & Mohrholz, V. Expanding oxygen-minimum zones on the tropical oceans. *Science* **320,** 655–658 (2008).
41. Reid, J. L. On the total geostrophic circulation of the Pacific ocean: flow patterns, tracers, and transports. *Prog. Oceanogr.* **39,** 263–352 (1997).
42. Karl, D. A sea of change: biogeochemical variability in the North Pacific Subtropical Gyre. *Ecosystems* **2,** 181–214 (1999).
43. Hare, E. P., Fogel, M. L., Stafford, T. W., Mitchell, A. D. & Hoering, T. C. The isotopic composition of carbon and nitrogen in individual amino acids isolated from modern and fossil proteins. *J. Archaeol. Sci.* **18,** 277–292 (1991).
44. Styring, A. K., Sealy, J. C. & Evershed, R. P. Resolving the bulk $\delta^{15}N$ values of ancient human and animal bone collagen via compound-specific nitrogen isotope analysis of constituent amino acids. *Geochim. Cosmochim. Acta* **74,** 241–251 (2010).

45. Germain, L. R., Koch, P. L., Harvey, J. T. & McCarthy, M. D. Nitrogen isotope fractionation in amino acids from harbor seals: implications for compound-specific trophic position calculations. *Mar. Ecol. Prog. Ser.* **482,** 265–277 (2013).
46. Gruber, N. *The Dynamics of the Marine Nitrogen Cycle and its Influence on Atmospheric CO_2 Variations* NATO Science Series Vol. 40, 97–148 (Springer, 2004).
47. Broek, T. A. B., Walker, B. D., Andreason, D. H. & McCarthy, M. D. High precision measurement of phenylalanine $\delta^{15}N$ values for environmental samples: a new approach coupling high-pressure liquid chromatography (HPLC) purification and elemental analysis-isotope ratio mass spectrometry (EA-IRMS). *Rapid Commun. Mass Spectrom.* **27,** 1–11 (2013).

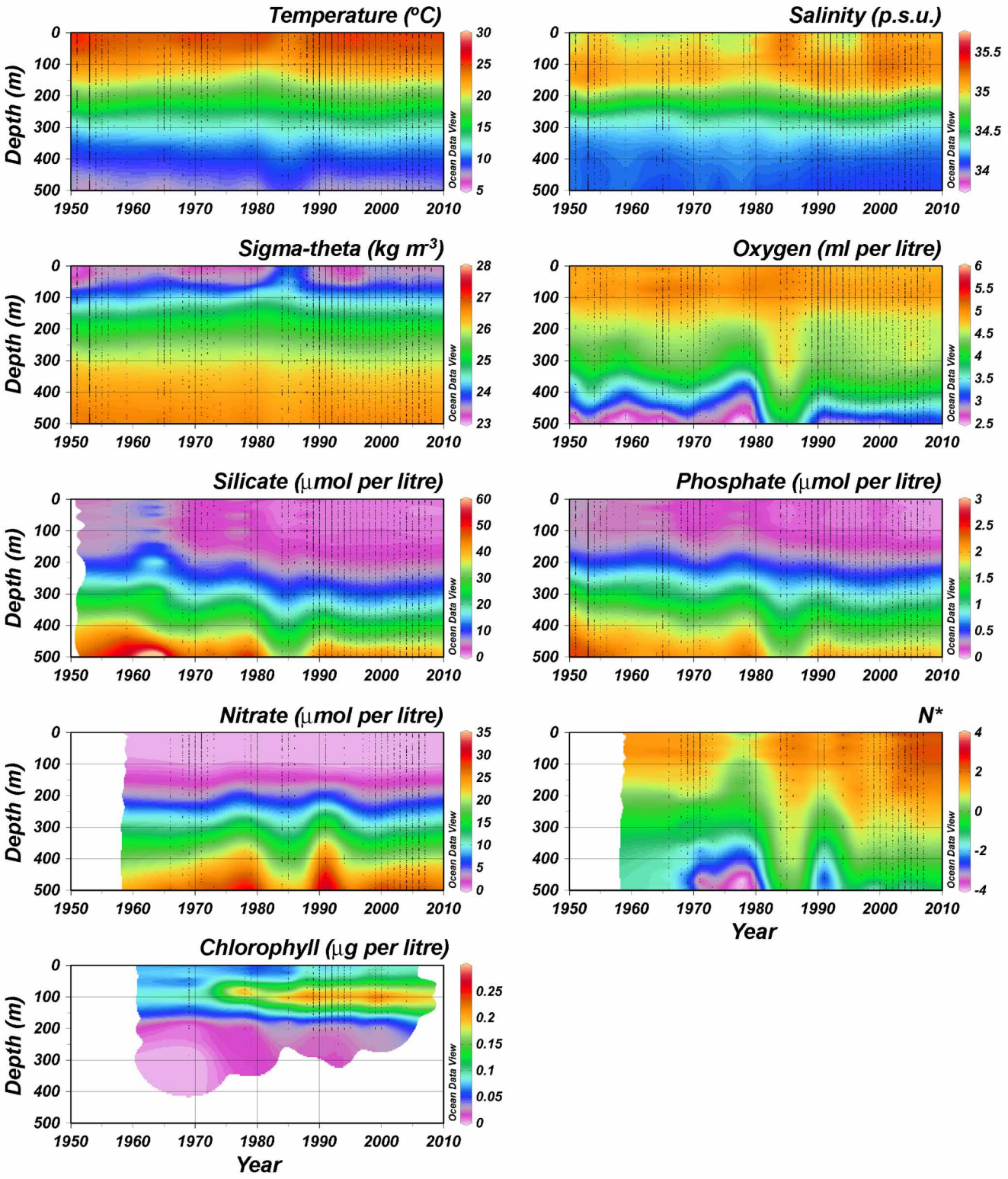

Extended Data Figure 1 | World Ocean Database 2009 instrumental records demonstrate physical and biological changes in the NPSG since 1950. Increasing salinity and temperature is accompanied by a strong decrease in silicate and phosphate nutrient concentrations, and an increase in N*. These data are consistent with the previously observed shift from a dominantly eukaryotic to dominantly prokaryotic (N_2-fixation) ecosystem in the NPSG[2,3,42]. Increasing rates of change with depth suggest large-scale changes in oceanographic circulation, consistent with expansion of the NPSG. Rates of change across separate depth bins are provided in Extended Data Table 1.

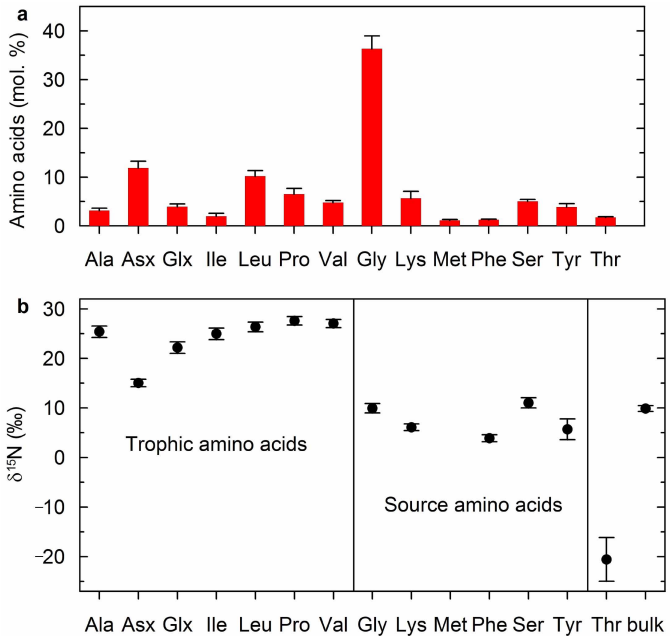

Extended Data Figure 2 | Distribution of amino-acid concentration and $\delta^{15}N_{aa}$ in *K. haumeaae*. **a**, Amino-acid mole per cent composition. **b**, $\delta^{15}N_{aa}$ data, showing two main groups: relatively $\delta^{15}N$-enriched 'trophic' amino acids (TrAA), and relatively lower-$\delta^{15}N$ 'source' amino acids (SrcAA). These patterns are very close to those of heterotrophic fresh biomass[18,19,21]. Together with low ΣV values (Table 1), this supports the use of $\delta^{15}N_{Phe}$ as a proxy for the $\delta^{15}N$ of exported production, and indicates that $\delta^{15}N$ values have not undergone any significant diagenetic alteration. Extremely low values of threonine (Thr) are consistent with previous observations[43,44], and this amino acid is now understood to be neither a trophic nor source amino acid[45]. Mean $\delta^{15}N_{bulk}$ is shown for context. Error bars represent 1 s.d. ($n = 20$).

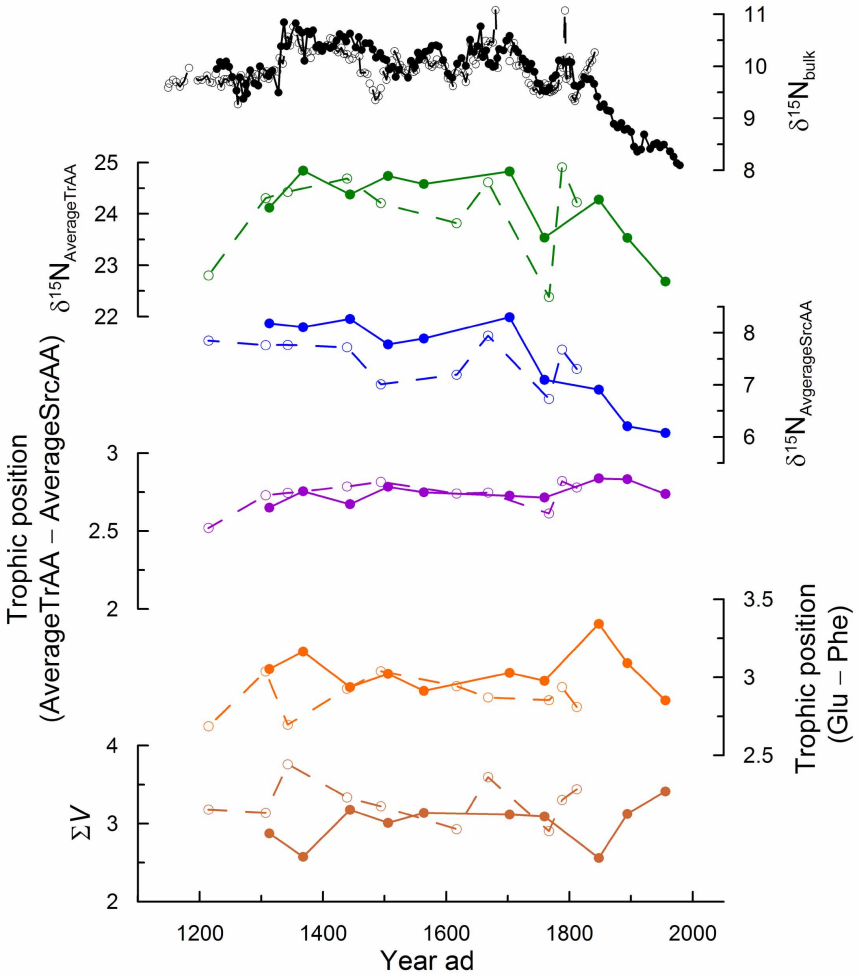

Extended Data Figure 3 | Timeseries of $\delta^{15}N_{aa}$ parameters in comparison to $\delta^{15}N_{bulk}$ from two *K. haumeaae* specimens from Makapuu. Closed symbols, specimen Ger9701; open symbols, specimen Ger9702. Trophic position and ΣV parameters are defined in Table 1.

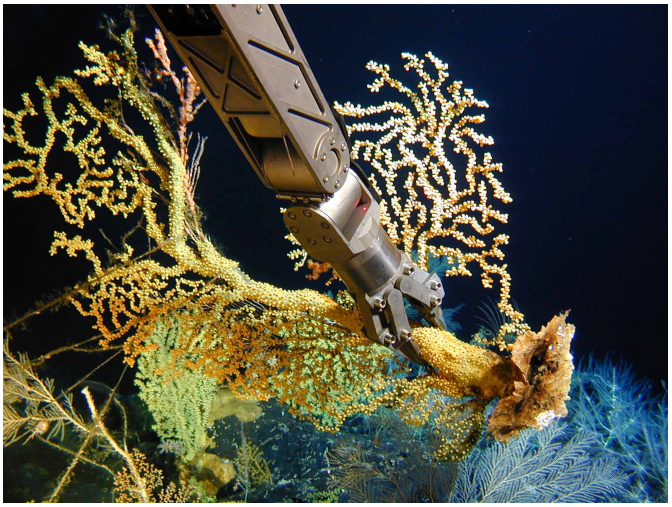

Extended Data Figure 4 | Example *K. haumeaae* colony photographed *in situ*. Photo credit: NOAA Hawaiian Undersea Research Laboratory, DSRV *Pisces* Pilots & Engineers, 2004.

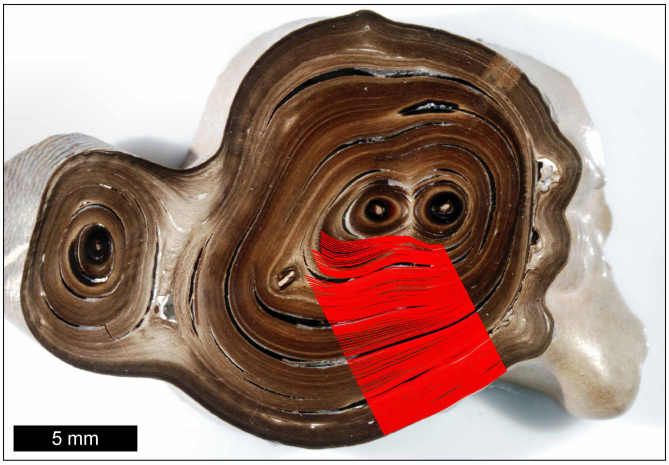

Extended Data Figure 5 | Example *K. haumeaae* skeletal cross-section. Specimen Ger9701 from Makapuu. Red lines indicate micromill transect.

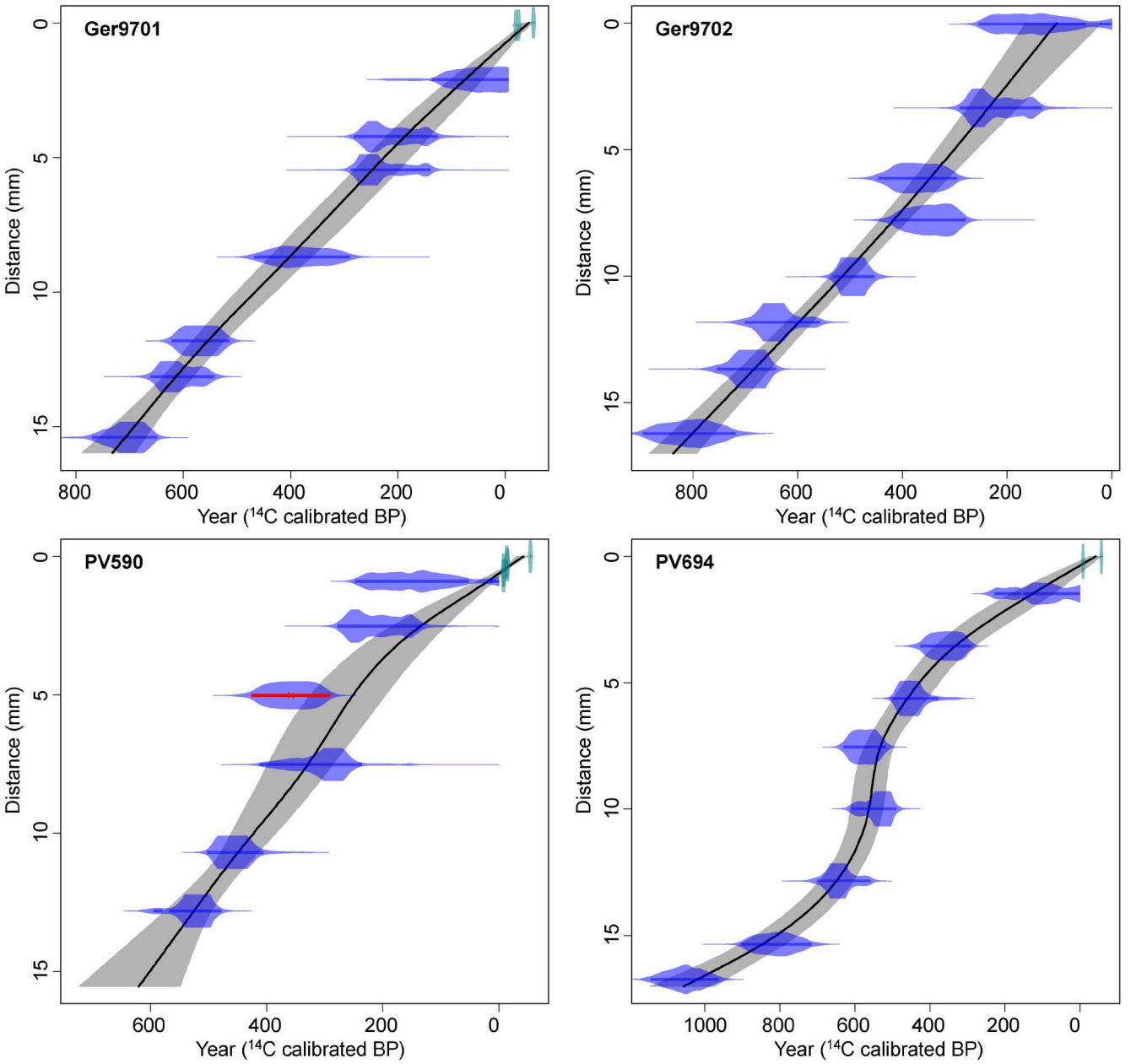

Extended Data Figure 6 | Radiocarbon age models. Blue-shaded areas represent conventional ^{14}C calibrated age distributions. Green-shaded areas are post-bomb (post-1950) age distributions. Black curves and grey-shaded regions represent spline fits with 95% confidence intervals, respectively. The average age model error is 45 years. Outliers (indicated in red) were excluded from age models owing to age reversals. The shape of the curves reflects variable growth rates in the four coral samples illustrated.

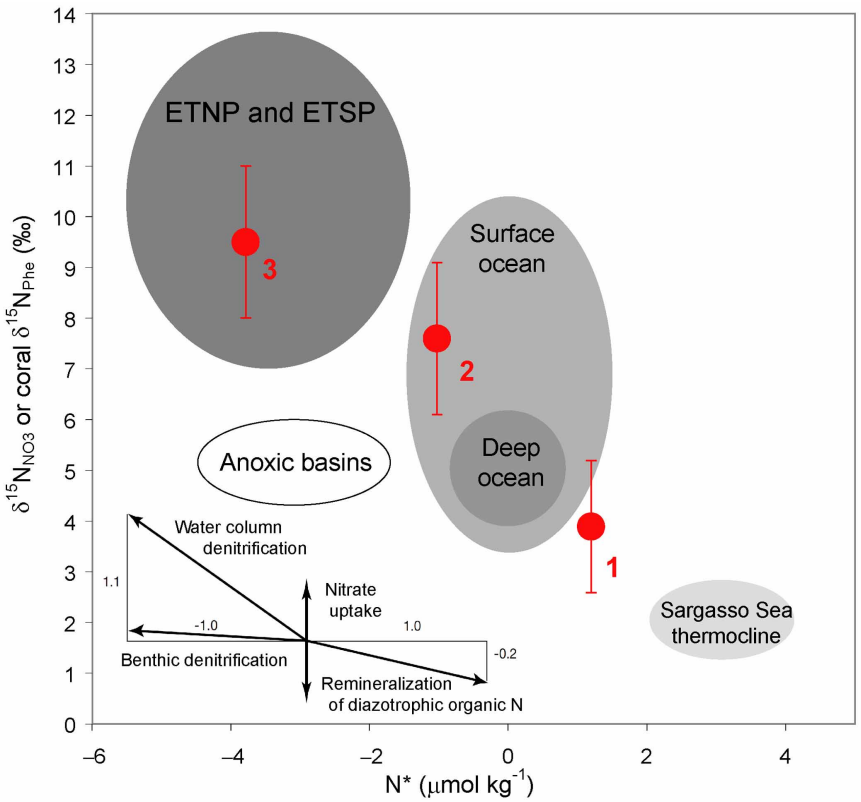

Extended Data Figure 7 | Relationship between $\delta^{15}N$ and N* across different oceanographic regions. The $\delta^{15}N_{NO3}$ is driven by isotopic fractionation processes of denitrification, nitrate uptake and remineralization of diazotrophic organic nitrogen (ETNP, Eastern Tropical North Pacific; ETSP, Eastern Tropical South Pacific; redrawn from ref. 46). Existing deep-sea coral $\delta^{15}N_{Phe}$ data (red points) closely follow the same overall pattern. Data points are: (1) Hawaii *K. haumeaae* (2 specimens, 20 measurements; this paper); (2) Northwest Atlantic *Primnoa resedaeformis* (2 specimens, 8 measurements[15]); (3) Monterey Bay *Isidella* sp. (1 specimen, 10 measurements[47]); Error bars show the total range of measurements. Corresponding values of N* are obtained from the nearest surface water grid point of the World Ocean Atlas 2009 (http://www.nodc.noaa.gov/OC5/WOA09/woa09data.html).

Extended Data Table 1 | World Ocean Database 2009 physical and chemical parameters

	0-150 m		151-300 m		301-500 m	
Parameter	Slope ± Std.Error	P value	Slope ± Std.Error	P value	Slope ± Std.Error	P value
Temperature (°C)	+0.004 ± 0.007	0.566	+0.017 ± 0.006	**0.009**	+0.007 ± 0.005	0.109
Salinity (p.s.u.)	+0.003 ± 0.001	**0.012**	+0.002 ± 0.001	**0.02**	−0.001 ± 0.000	**0.005**
Sigma-theta (kg m^{-3})	+0.001 ± 0.003	0.656	−0.002 ± 0.001	**0.031**	−0.002 ± 0.001	**0.008**
Oxygen (ml per litre)	−0.001 ± 0.001	0.342	+0.003 ± 0.002	0.062	+0.013 ± 0.005	**0.016**
Silicate (μmol per litre)	−0.074 ± 0.023	**0.003**	−0.121 ± 0.051	**0.022**	−0.233 ± 0.097	**0.021**
Phosphate (μmol per litre)	−0.004 ± 0.001	**<0.001**	−0.006 ± 0.001	**0.001**	−0.008 ± 0.002	**0.001**
Nitrate (μmol per litre)	−0.004 ± 0.002	0.071	−0.004 ± 0.029	0.888	−0.007 ± 0.060	0.910
N*	+0.035 ± 0.011	**0.004**	+0.047 ± 0.014	**0.002**	+0.064 ± 0.031	**0.054**
Chlorophyll (μg per litre)	+0.002 ± 0.001	**0.014**	+0.001 ± 0.000	**0.006**	NA	NA

Changes in the parameters in the NPSG are shown from 1950 to 2010, across multiple depth bins. Boldface *P* values indicate statistically significant trends at the $P < 0.05$ level. Sigma-θ is the density of sea water at a reference level of 0 dbar (that is, at a depth of 0 m). NA, not available.

Extended Data Table 2 | *K. haumeaae* radiocarbon data

Coral	Location	CAMS ID	Sample	Distance (mm)	$\delta^{13}C$	Fraction modern	Error	$D^{14}C$	Error	^{14}C Age	Error
Ger9701	Makapuu	156055	1	0.10	−16.9	1.1138	0.0042	113.8	4.2	>Modern	
		156056	20	2.12	−15.7	0.9482	0.0029	−51.8	2.9	425	25
		156057	41	4.24	−15.6	0.9339	0.0035	−66.1	3.5	550	30
		156058	52	5.47	−15.7	0.9321	0.0028	−67.9	2.8	565	25
		156059	81	8.72	−16.0	0.9147	0.0046	−85.3	4.6	715	45
		156060	108	11.84	−16.1	0.8884	0.0028	−111.6	2.8	950	25
		156061	121	13.17	−16.4	0.8816	0.0029	−118.4	2.9	1015	30
		156062	141	15.43	−16.3	0.8684	0.0029	−131.6	2.9	1135	30
Ger9702	Makapuu	153722	4z	0.04	−15.7	0.9414	0.0039	−58.6	3.9	485	35
		153723	40	3.35	−15.6	0.9334	0.0034	−66.6	3.4	555	30
		156064	64	6.12	−15.6	0.9170	0.0030	−83.0	3.0	695	30
		153724	80	7.78	−16.1	0.9204	0.0030	−79.6	3.0	665	30
		156065	102	10.02	−16.4	0.9006	0.0026	−99.4	2.6	840	25
		153725	120	11.82	−16.2	0.8780	0.0037	−122.0	3.7	1045	35
		156066	138	13.67	−16.4	0.8711	0.0029	−128.9	2.9	1110	30
		153726	160	16.21	−16.8	0.8583	0.0037	−141.7	3.7	1225	35
PV590	Cross Seamount	157079	2	0.20	−17.0	1.0736	0.0044	73.6	4.4	>Modern	
		157080	3	0.30	−17.4	1.0855	0.0038	85.5	3.8	>Modern	
		157081	5	0.50	−16.7	0.9714	0.0028	−28.6	2.8	>Modern	
		157082	7	0.70	−16.7	0.9592	0.0028	−40.8	2.8	335	25
		157083	9	0.90	−16.6	0.9419	0.0027	−58.1	2.7	480	25
		157084	25	2.52	−16.5	0.9347	0.0027	−65.3	2.7	540	25
		157085	50	5.02	−16.1	0.9186	0.0027	−81.4	2.7	680	25
		157086	75	7.52	−15.5	0.9264	0.0038	−73.6	3.8	615	35
		157087	106	10.69	−16.4	0.9073	0.0024	−92.7	2.4	780	25
		157088	127	12.81	−16.3	0.8956	0.0026	−104.4	2.6	885	25
PV694	French Frigate Shoals	159298	3	0.20	−16.5	0.9699	0.0031	−30.1	3.1	>Modern	
		159299	15	1.47	−15.7	0.9441	0.0030	−55.9	3.0	460	30
		159300	33	3.55	−15.8	0.9186	0.0028	−81.4	2.8	680	25
		159301	52	5.62	−16.3	0.9082	0.0030	−91.8	3.0	775	30
		159302	71	7.54	−16.1	0.8884	0.0030	−111.6	3.0	950	30
		159303	92	9.99	−16.5	0.8941	0.0029	−105.9	2.9	900	30
		159304	112	12.84	−16.5	0.8779	0.0037	−122.1	3.7	1045	35
		159305	152	15.34	−16.6	0.8579	0.0039	−142.1	3.9	1230	40
		159433	132	16.74	−16.5	0.8326	0.0027	−167.4	2.7	1470	30

Note that specimen Ger9702 was collected dead; the other three specimens were collected alive. CAMS, Center for Accelerator Mass Spectrometry.